



This is a repository copy of *Age, sex, and lung volume dependence of dissolved xenon-129 MRI gas exchange metrics*.

White Rose Research Online URL for this paper:

<https://eprints.whiterose.ac.uk/212419/>

Version: Published Version

---

**Article:**

Collier, G.J. [orcid.org/0000-0002-1874-4775](https://orcid.org/0000-0002-1874-4775), Smith, L.J., Saunders, L.C. [orcid.org/0000-0002-1080-9861](https://orcid.org/0000-0002-1080-9861) et al. (7 more authors) (2024) Age, sex, and lung volume dependence of dissolved xenon-129 MRI gas exchange metrics. *Magnetic Resonance in Medicine*. ISSN 0740-3194

<https://doi.org/10.1002/mrm.30133>

---

**Reuse**

This article is distributed under the terms of the Creative Commons Attribution (CC BY) licence. This licence allows you to distribute, remix, tweak, and build upon the work, even commercially, as long as you credit the authors for the original work. More information and the full terms of the licence here:

<https://creativecommons.org/licenses/>







**Takedown**

If you consider content in White Rose Research Online to be in breach of UK law, please notify us by emailing [eprints@whiterose.ac.uk](mailto:eprints@whiterose.ac.uk) including the URL of the record and the reason for the withdrawal request.



[eprints@whiterose.ac.uk](mailto:eprints@whiterose.ac.uk)  
<https://eprints.whiterose.ac.uk/>

# Age, sex, and lung volume dependence of dissolved xenon-129 MRI gas exchange metrics

Guilhem J. Collier<sup>1,2</sup>  | Laurie J. Smith<sup>1</sup> | Laura C. Saunders<sup>1</sup>  | Andrew J. Swift<sup>1,2</sup> | Helen Marshall<sup>1,2</sup> | Neil J. Stewart<sup>1,2</sup>  | Graham Norquay<sup>1</sup>  | Paul J. C. Hughes<sup>1</sup>  | A. A. Roger Thompspon<sup>1</sup>  | Jim M. Wild<sup>1,2</sup>

<sup>1</sup>POLARIS, Division of Clinical Medicine, School of Medicine & Population Health, University of Sheffield, Sheffield, UK

<sup>2</sup>Insigneo Institute, University of Sheffield, Sheffield, UK

## Correspondence

Guilhem J. Collier, MRI Unit, University of Sheffield, C Floor, Royal Hallamshire Hospital, Glossop Road, Sheffield, S10 2JF, UK.

Email: [g.j.collier@sheffield.ac.uk](mailto:g.j.collier@sheffield.ac.uk)

## Funding information

Engineering and Physical Sciences Research Council, Grant/Award Number: EP/X025187/1; National Institute for Health and Care Research, Grant/Award Number: COV-LT2-0049; Medical Research Council, Grant/Award Number: MR/M008894/1

## Abstract

**Purpose:** To characterize the dependence of Xe-MRI gas transfer metrics upon age, sex, and lung volume in a group of healthy volunteers.

**Methods:** Sixty-five subjects with no history of chronic lung disease were assessed with <sup>129</sup>Xe-MRI using a four-echo 3D radial spectroscopic imaging sequence and a dose of xenon titrated according to subject height that was inhaled from a lung volume of functional residual capacity (FRC). Imaging was repeated in 34 subjects at total lung capacity (TLC). Regional maps of the fractions of dissolved xenon in red blood cells (RBC), membrane (M), and airspace (Gas) were acquired at an isotropic resolution of 2 cm, from which global averages of the ratios RBC:M, RBC:Gas, and M:Gas were computed.

**Results:** Data from 26 males and 36 females with a median age of 43 y (range: 20–69 y) were of sufficient quality to analyze. Age ( $p = 0.0006$ ) and sex ( $p < 0.0001$ ) were significant predictors for RBC:M, and a linear regression showed higher values and steeper decline in males:  $\text{RBC:M}(\text{Males}) = -0.00362 \times \text{Age} + 0.60$  ( $p = 0.01$ ,  $R^2 = 0.25$ );  $\text{RBC:M}(\text{Females}) = -0.00170 \times \text{Age} + 0.44$  ( $p = 0.02$ ,  $R^2 = 0.15$ ). Similarly, age and sex were significant predictors for RBC:Gas but not for M:Gas. RBC:M, M:Gas and RBC:Gas were significantly lower at TLC than at FRC (plus inhaled volume), with an average 9%, 30% and 35% decrease, respectively.

**Conclusion:** Expected age and sex dependence of pulmonary function concurs with <sup>129</sup>Xe RBC:M imaging results, demonstrating that these variables must be considered when reporting Xe-MRI metrics. Xenon doses and breathing maneuvers should be controlled due to the strong dependence of Xe-MRI metrics upon lung volume.

## KEYWORDS

ageing, hyperpolarized <sup>129</sup>Xe, lung, lung volume, spectroscopic imaging

## 1 | INTRODUCTION

Lung MRI utilizing hyperpolarized (HP)  $^{129}\text{Xe}$  has experienced renewed interest due to the advancements in the efficient production of large quantities of HP gas<sup>1</sup> and improvements of dissolved xenon imaging techniques with their application to assess gas exchange abnormalities in pulmonary diseases such as pulmonary fibrosis,<sup>2,3</sup> chronic obstructive lung disease (COPD)<sup>4,5</sup> and recently coronavirus disease 2019 (COVID-19).<sup>6–8</sup> Due to the discrete MR spectral peaks of  $^{129}\text{Xe}$  in the different lung compartments: alveolar gas, dissolved in lung parenchyma and blood plasma (membrane, M) and in red blood cells (RBC), it is possible to acquire images of gas transfer by calculating ratio maps of  $^{129}\text{Xe}$  MR signal from the different compartments. Multiple dissolved  $^{129}\text{Xe}$  imaging techniques have been implemented, including 1-point Dixon,<sup>2</sup> multi point IDEAL,<sup>9,10</sup> CSI<sup>11</sup> and xenon transfer contrast.<sup>12</sup> Most of these techniques are able to generate 3D maps of tissue uptake (M:Gas),  $^{129}\text{Xe}$  transfer to the blood (RBC:Gas) and RBC:M while keeping the acquisition time within a 15 s breath-hold. These metrics, together with the measurement of the cardiac output-driven RBC signal oscillation (RBCOsc), also acquired during the breath-hold,<sup>13–15</sup> have shown sensitivity and specificity to a diverse number of cardiopulmonary diseases.<sup>5</sup> However, normative data sets from healthy subjects across a broad age range are needed before wide-ranging clinical conclusions can be drawn<sup>16</sup> and these are currently lacking.

Dissolved  $^{129}\text{Xe}$  imaging outcome measurements depend on sequence parameters such as the flip angle, TE, and TR<sup>17</sup>. An attempt to harmonize methods to acquire HP  $^{129}\text{Xe}$  lung MRI has been published recently<sup>18</sup> with the goal of reducing inter-site variability of the measurements. However, little has been published on the effects of lung volume, sex and age on  $^{129}\text{Xe}$  gas transfer ratios. Age, sex, and lung volume dependence of gas transfer tests are known physiological phenomena. In clinical practice, the pulmonary physiology gold standard test of gas exchange across the lung is the measurement of transfer factor for carbon monoxide ( $T_{\text{LCO}}$ , and its constant  $K_{\text{CO}}$ ). To clinically assess  $T_{\text{LCO}}$ , the respiratory societies of Europe and America (ERS and ATS) recommend using the standardized predictive equations for the Caucasian population, recently published by the global lung initiative group, which accounts for differences in age, sex and height.<sup>19</sup> A HP  $^{129}\text{Xe}$  MRI gas exchange model has been recently published<sup>20</sup> that directly links the  $^{129}\text{Xe}$  imaging ratios with  $K_{\text{CO}}$  and  $T_{\text{LCO}}$ , and it is therefore expected that the  $^{129}\text{Xe}$  imaging outcome parameters would also be dependent on population demographics.

Age dependence of the lung septal thickness inferred from  $^{129}\text{Xe}$  MR CSSR measurements have already been

reported in a cohort of 10 healthy volunteers,<sup>21</sup> showing an increase in thickness with age. More recently, the impact of age from childhood to adulthood on healthy reference distributions of  $^{129}\text{Xe}$  gas exchange metrics in a cohort of 30 healthy subjects over an age range of 5–68 y has been published,<sup>22</sup> using generalized additive models for location, scale and shape (GAMLSS). While the results show significant differences of the distribution of  $^{129}\text{Xe}$  gas exchange metrics with age, the study population was too small to introduce additional variables such as sex, height, and weight. Dissolved xenon tissue uptake and transfer to the blood have been shown to decrease significantly with increasing lung volume.<sup>23,24</sup> Subsequently, dosing the inhaled gas according to subject's height or total lung capacity has been recommended.<sup>18</sup>

In this study, we hypothesized that HP  $^{129}\text{Xe}$  spectroscopic imaging gas exchange metrics would not only decrease with increasing age and lung volume but would also be dependent upon additional demographics such as sex, height, weight, and body mass index (BMI).

## 2 | METHODS

### 2.1 | Participants

All imaging protocols were performed under the approval of the UK National Research Ethics Committee (REC reference numbers 17/LO/0725 and 21/SC/0398) and University of Sheffield ethics UOS030529. Sixty-five healthy subjects with no known respiratory conditions and spanning an age range of 20–69 y were recruited and provided written informed consent. Current smokers and participants with significant smoking history (>10 pack-years) were excluded. Among these 65 subjects, 41 never tested positive for COVID-19 while 24 of them had COVID-19 at least 3 mo or more prior to the imaging session. Post-COVID-19 subjects did not have ongoing symptoms after the acute phase of COVID-19 and hospitalization during the acute phase was an exclusion criterion. All subjects were imaged in the supine position at a lung volume of functional residual capacity plus a bag of HP  $^{129}\text{Xe}$  dose corresponding to the end-inspiratory tidal volume (EIVt). Thirty-four had an additional scan at total lung capacity (TLC) in order to evaluate the influence of subject demographics and lung volume on dissolved  $^{129}\text{Xe}$  imaging measurements.

### 2.2 | MRI acquisition

MR imaging was conducted on a 1.5T GE HDx scanner using a flexible quadrature transmit/receive vest RF coil.

Enriched hyperpolarized  $^{129}\text{Xe}$  doses were produced using a spin-exchange optical pumping polarizer to a polarization level of  $\sim 30\%$ .<sup>25</sup> Following tidal expiration, the subjects were instructed to breathe in the 0.8–1 L doses (determined by patient height, see Table S1) of pure HP  $^{129}\text{Xe}$  from a Tedlar bag. To control the lung inflation level and reproducibility, subjects were trained before the actual dissolved xenon imaging sequence and a nose clip was used to avoid nasal respiration. Imaging at EIVt was then performed during a 14 s breath-hold following inhalation of the dose of gas. Thirty-four out of the 65 subjects were additionally instructed to repeat imaging at TLC by topping up their lungs with room air following the inhalation of the gas. To assess reproducibility, eight subjects were scanned at EIVt three times during the same day: twice during the same imaging session within a 15 min interval and one additional time,  $\sim 4\text{--}6$  h after the initial measurement.

The dissolved xenon imaging sequence is an updated version of the four-echo flyback 3D radial spectroscopic imaging method described previously in Ref. 3. Briefly, the main updates are the implementation of a frequency-tailored RF excitation pulse previously described in<sup>11</sup> that excites the gas phase with 1% of the flip angle applied to the dissolved phase compartment. This allowed for a more efficient sampling time by removing the need for interleaved RF excitation of gas and dissolved phase  $^{129}\text{Xe}$ , hence allowing increased number of radial projections from 332 to 934. Additionally, the TR has been shortened to 15 ms and the flip angle reduced from 40 to 22 degrees to match the recommended imaging parameters of the  $^{129}\text{Xe}$  MRI clinical trials consortium.<sup>18</sup> Finally, the calibration pulse-acquire spectrum required to estimate the frequency positions and transverse relaxation time  $T_2^*$  of each resonance has been inserted at the start of the imaging sequence. These estimates are used as prior information to improve the chemical shift reconstruction and are derived by performing a triple Lorentzian fit of the data in the frequency domain.<sup>26</sup> This latter addition removed the use of a separate calibration dose and sequence in the imaging protocol. The remaining imaging parameters were kept the same and were: 40 cm FOV, 31.25 kHz bandwidth, 2 cm isotropic acquired resolution reconstructed to 1.25 cm isotropic image resolution, 934 radial projections, TEs of 0.57/1.27/1.97/2.67 ms, 20 dummy RF pulses at the start of the sequence to reach steady state (and acquire calibration spectra), 14 s acquisition time.

### 2.3 | Data analysis

Raw data were analyzed offline using MATLAB (MathWorks, Natick, Massachusetts, USA). The chemical

shift separation was performed in k-space using matrix inversion<sup>3</sup> and prior knowledge of the three resonance frequencies and decay times estimated from a triple Lorentzian fit<sup>26</sup> of the average of the 20 frequency spectra acquired at the start of the sequence. After regridding and a Fourier transform of each k-space (Gas, M, RBC), ratio maps of RBC:M, RBC:Gas and M:Gas were produced after correcting signal amplitude for differences in  $T_2^*$  decays during readout and flip angles between gas and dissolved xenon. Global and regional averages of lung gas exchange (anterior/posterior, inferior/middle/superior and proximal/distal) were derived for each subject. To assess the degree of heterogeneity, coefficients of variation within the gas exchange ratio maps, ( $CV_{\text{RBC:M}}$ ,  $CV_{\text{RBC:Gas}}$ ,  $CV_{\text{M:Gas}}$ ) were computed. In addition, the amplitude of the cardiogenic oscillation of the RBC signal (RBCOsc)<sup>13</sup> during the 14 s breath-hold was also derived from the first point ( $k_0$ ) of the RBC k-space radial projections. Example spectra, derivation of RBCOsc and representative RBC:M maps are shown in Figure 1 for two subjects from this study.

Spearman correlations were computed between the dissolved  $^{129}\text{Xe}$  imaging outcome metrics and age, weight, height, and BMI. Multiple linear regression was also performed between each major  $^{129}\text{Xe}$  imaging outcome variable (average gas exchange ratios, CVs, and RBCOsc) and the demographic metrics which were significantly correlated individually, plus sex. The parameters included in the multiple linear regression model were adjusted to exclude dependent variables and maximize the adjusted  $R^2$  while simultaneously keeping only significant predictors. From the linear regression equations, individual percent predicted values were derived. Z-scores were then computed using the standard deviation of the distribution of percent predicted values. Wilcoxon paired t-tests and Friedman paired analysis of variance (ANOVA) with Dunn's multiple comparison tests were used to analyze regional differences. Wilcoxon paired t-tests were performed to study the differences between imaging markers at EIVt and TLC. Intra- and inter-imaging session reproducibility was assessed with Bland–Altman and intraclass correlation (ICC) analysis. The two-way mixed, single measures, agreement ICC (A,1) was used and computed with IBM SPSS statistics 27 (SPSS, New York, USA) while all other statistical tests were performed in GraphPad Prism (V9.0, San Diego, CA, USA).

### 3 | RESULTS

Three datasets out of the 65 subjects had to be discarded due to insufficient dissolved xenon image quality (two) and incidental imaging finding (one), resulting in

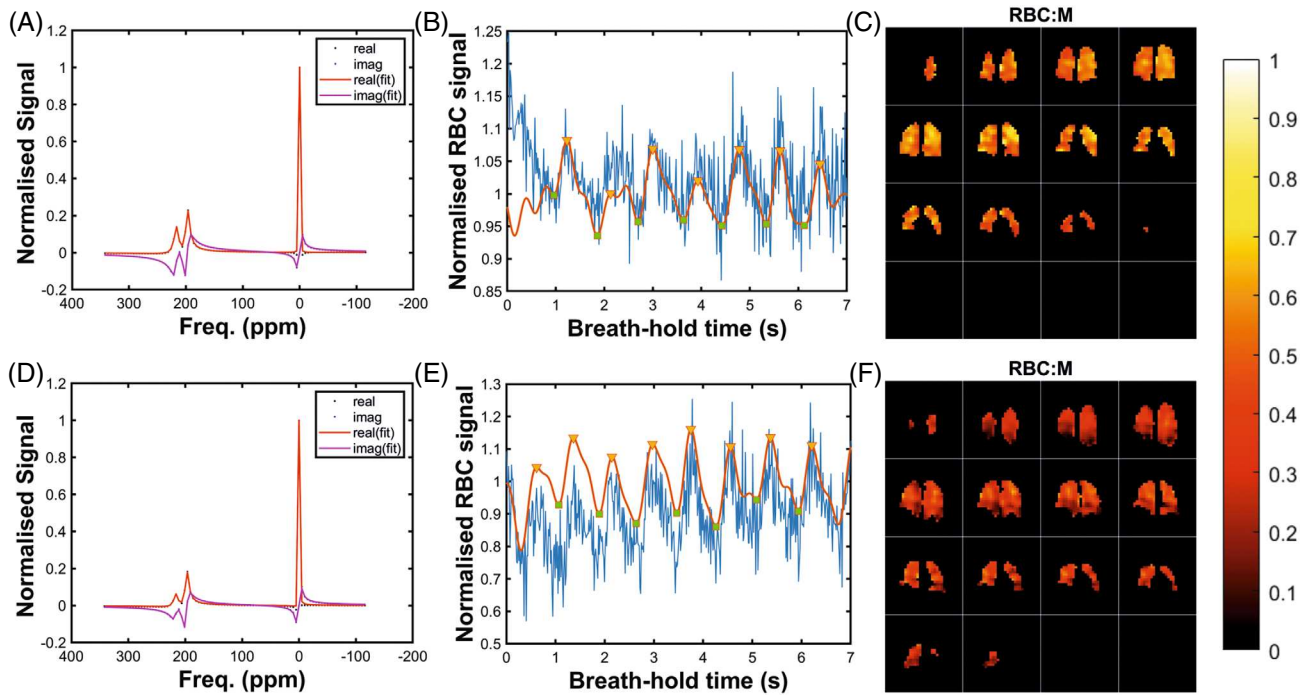


**FIGURE 1** Representative data for a young healthy male (30 y, top) and an older female (60 y, bottom). (A, D) average frequency spectra from the 20 FIDs acquired at the start of the imaging sequence with their corresponding fit of the real and imaginary components using a triple Lorentzian model. Center frequencies and  $T_2^*$  decays from the fit of each peak are used to perform the chemical shift separation in the k-space before re-gridding. (B, E) Normalized  $^{129}\text{Xe}$  RBC signal evolution during the first 7 s of the imaging acquisition. The signal comes from the k-space center of each radial projection after performing the CS separation and applying a correction from a bi-exponential fit of the  $^{129}\text{Xe}$  M signal decay. After filtering the raw signal (blue line) with a band pass filter (red line), a peak detection algorithm is used to detect maxima (yellow triangles) and minima (green squares) and calculate an average peak to peak amplitude oscillation for RBC signal (RBCOsc). (C, F) Corresponding ratio maps of  $^{129}\text{Xe}$  RBC images/ $^{129}\text{Xe}$  M images (RBC:M) after re-gridding and Fourier transform of dissolved  $^{129}\text{Xe}$  and  $^{129}\text{Xe}$  gas signals in the lung.

62 included subjects for the age dependency analysis, 34 paired data sets for the lung volume comparison, and 8 data sets for the reproducibility analysis. Subject demographics, including smoking history and post-COVID-19 infection status are provided in the Tables S2, S3, and S4 and summarized below (reported as median and first and third quartile [Q1–Q3]): 26 males/36 females, age = 43 (33–54) y, weight = 74 (65–82) kg, height = 172 (163–183) cm, BMI = 24.8 (22.3–26.6) kg/m<sup>2</sup>. The new implementation of the four-echo radial flyback imaging sequence produced a successful chemical shift separation of gas, RBC and membrane signals and images of similar quality to those described in Ref. 3 were obtained. Example representative RBC:M maps for two healthy volunteers can be seen in Figure 1C,F. Thanks to the implementation of a frequency-tailored RF pulse with controlled RF excitation on gas and dissolved xenon resonances, alongside a shorter TR of 15 ms, the number of radial projections could be increased from 332 to 934. This modification led to complete k-space sampling, thereby eliminating radial streak artifact in the images.

### 3.1 | Reproducibility analysis

Figure 2 shows the Bland–Altman plots of the inter- and intra-session measurement of RBC:M, RBC:Gas, M:Gas and RBCOsc. As expected, the measurements were more reproducible within the same imaging session with ICC values of 0.983, 0.748, 0.926, and 0.670, respectively. The results from Bland–Altman and intraclass correlation analyses for both inter- and intra-sessions are summarized in Table 1. The global RBC:M ratio was the most reproducible xenon gas exchange imaging parameter (tightest 95% limits of agreement and highest ICC values). On the contrary, RBCOsc had poor reproducibility with a broad 95% confidence interval on the intra- and inter-sessions ICC values.

### 3.2 | Age and sex dependence

The median and interquartile range values of the dissolved  $^{129}\text{Xe}$  imaging outcome metrics over the 62

FIGURE 2

Bland–Altman plots (% difference vs. average) of RBC:M (A), RBC:Gas (B), M:Gas (C), and RBCOsc (D) as a measurement of intra-session (black circles) and inter-session/intra-day (red squares) reproducibility for the main dissolved xenon imaging output parameters. The dashed lines show the mean differences and the dotted lines represent the 95% confidence intervals.

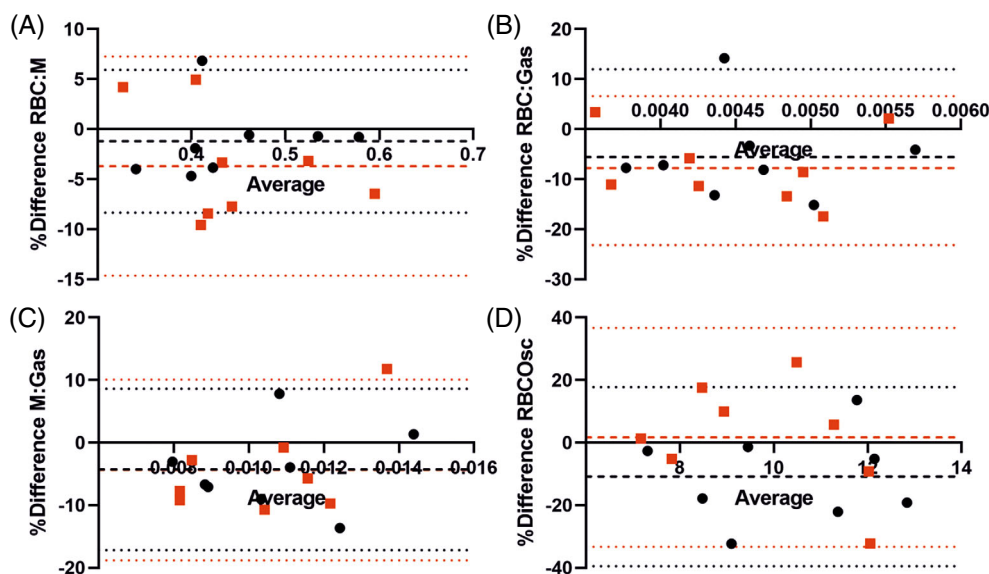


TABLE 1 Bland–Altman and ICC analysis results for the intra- and inter-session reproducibility study.

Parameter	Imaging outcome parameter	Bland–Altman analysis: bias [95% limits of agreement]	Intraclass correlation analysis: ICC ( <i>p</i> -value, [95% confidence interval])
Intra-sessions	RBC:M	−1.2 [−8.3, 5.9]	0.983 ( <i>p</i> < 0.001, [0.924–0.996])
	RBC:Gas	−5.6 [−23.1, 12.0]	0.748 ( <i>p</i> = 0.007, [0.200–0.943])
	M:Gas	−4.3 [−17.2, 8.6]	0.926 ( <i>p</i> < 0.001, [0.676–0.985])
	RBCOsc (%)	−10.9 [−39.5, 17.8]	0.670 ( <i>p</i> = 0.02, [0.060–0.922])
Inter-sessions	RBC:M	−3.7 [−14.6, 7.3]	0.941 ( <i>p</i> < 0.001, [0.662–0.989])
	RBC:Gas	−7.8 [−22.1, 6.6]	0.796 ( <i>p</i> = 0.02, [0.088–0.960])
	M:Gas	−4.4 [−18.8, 10.1]	0.905 ( <i>p</i> < 0.001, [0.631–0.980])
	RBCOsc (%)	1.7 [−33.3, 36.7]	0.917 ( <i>p</i> = 0.05, [−0.154–0.912])

Note: The two-way mixed, single measures, agreement ICC (A,1) was used.

subjects are provided in Table 2 together with the results of the multiple linear regression analyses. Age (*p* = 0.0006) and sex (*p* < 0.0001) were significant predictors for RBC:M (adjusted  $R^2$  of 0.36). RBC:M was significantly lower in women and a separate linear regression analysis showed a steeper decline of RBC:M with age in men than in women (see Figure 3A, RBC:M (M) =  $-0.00362 \times \text{Age} + 0.60$ ,  $R^2 = 0.25$ , *p* = 0.01 vs. RBC:M (F) =  $-0.00170 \times \text{Age} + 0.44$ ,  $R^2 = 0.15$ , *p* = 0.02) with predicted values dropping by 34% (from 0.53 to 0.35) in men and 21% (from 0.41 to 0.32) in women over the age range of 20–70 yr. Using this set of linear equations for predicted RBC:M in males and females, z-scores were derived. The distribution of z-scores (e.g., Figure 3B) passed the D'Agostino-Pearson omnibus normality test.

Age (*p* = 0.002) and sex (*p* = 0.0007) were also significant predictors for RBC:Gas (adjusted  $R^2$  of 0.27) with significantly higher values for men.

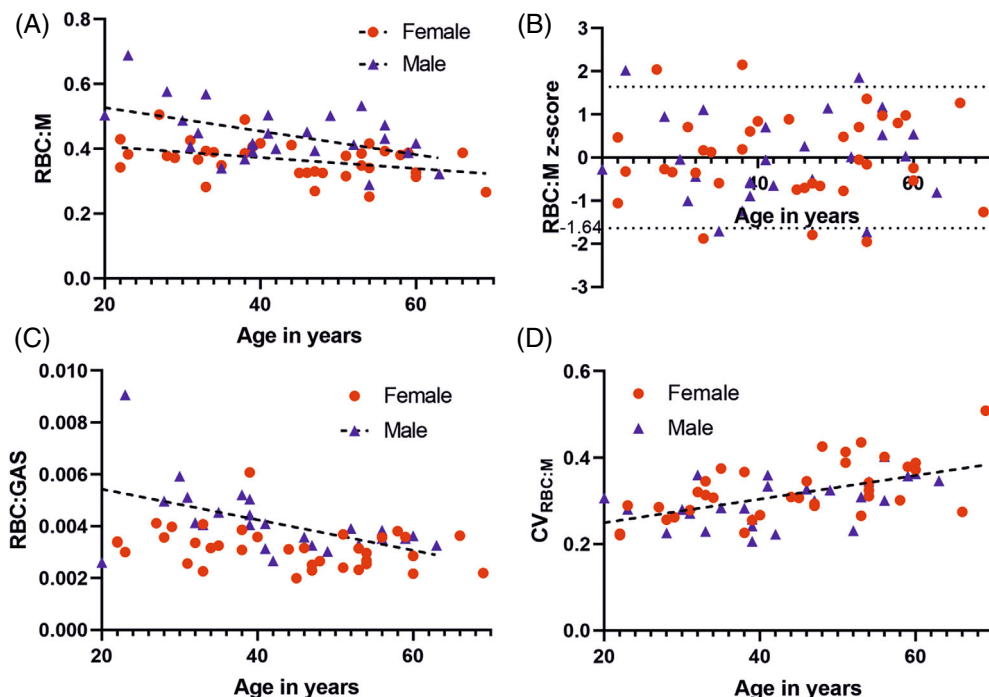
However, when male and female cohorts were separated, age was only significantly correlated with RBC:Gas in the male cohort (Figure 3C, RBC:gas (M) =  $-0.0000591 \times \text{Age} + 0.00662$ ,  $R^2 = 0.28$ , *p* = 0.006 versus *p* = 0.09 for the female cohort, median [Q1, Q3] RBC:Gas (F) = 0.0032 [0.0025, 0.0036]). There were no significant predictors for M:Gas or RBCOsc.  $CV_{\text{RBC:M}}$  (See Figure 3D) and  $CV_{\text{RBC:Gas}}$  increased significantly with age ( $CV_{\text{RBC:M}} = 0.0027 \times \text{Age} + 0.1952$ ,  $R^2 = 0.30$ , *p* < 0.0001 and  $CV_{\text{RBC:Gas}} = 0.0021 \times \text{Age} + 0.3113$ ,  $R^2 = 0.13$ , *p* = 0.004, respectively), suggesting an increase in gas exchange heterogeneity within the lung with age. While height and weight were individually significantly correlated with  $CV_{\text{M:Gas}}$ , sex was the only significant predictor for  $CV_{\text{M:Gas}}$  (*p* < 0.0001) in the multi linear regression analysis due to the fact that sex, height and weight were dependent variables. The same reason explains the disappearance of a number of significant predictors in the

TABLE 2 Lung imaging results in the 62 healthy volunteers.

Imaging outcome parameter	Median [IQR]	Correlation analysis (Spearman $r$ , $p$ ). ** denotes $p < 0.05$ .	Multiple linear regression analysis ( $p$ and global adjusted $R^2$ )
RBC:M	0.39 [0.34, 0.43]	Age ( $-0.34$ , $p = 0.007$ )* Height ( $0.38$ , $p = 0.002$ )* Weight ( $0.12$ , $p = 0.37$ ) BMI ( $-0.23$ , $p = 0.08$ )	Age ( $p = 0.0006$ ) and sex ( $p < 0.0001$ ), adj. $R^2 = 0.36$
RBC:Gas	0.0034 [0.0028, 0.0040]	Age ( $-0.34$ , $p = 0.008$ )* Height ( $0.43$ , $p = 0.001$ )* Weight ( $0.29$ , $p = 0.02$ )* BMI ( $0.01$ , $p = 0.96$ )	Age ( $p = 0.002$ ) and sex ( $p = 0.0007$ ), adj. $R^2 = 0.27$
M:Gas	0.0089 [0.0076, 0.0099]	Age ( $-0.12$ , $p = 0.35$ ) Height ( $0.21$ , $p = 0.11$ ) Weight ( $0.23$ , $p = 0.08$ ) BMI ( $0.17$ , $p = 0.18$ )	NA
RBC:Sc (%)	13.7 [12, 15.7]	Age ( $0.22$ , $p = 0.13$ ) Height ( $-0.06$ , $p = 0.69$ ) Weight ( $0.07$ , $p = 0.62$ ) BMI ( $0.21$ , $p = 0.15$ )	NA
CV <sub>RBC:M</sub>	0.31 [0.27, 0.36]	Age ( $0.54$ , $p < 0.0001$ )* Height ( $-0.12$ , $p = 0.36$ ) Weight ( $0.08$ , $p = 0.53$ ) BMI ( $0.24$ , $p = 0.06$ )	Age ( $p < 0.0001$ ), adj. $R^2 = 0.29$
CV <sub>RBC:Gas</sub>	0.38 [0.34, 0.47]	Age ( $0.33$ , $p = 0.009$ )* Height ( $-0.01$ , $p = 0.93$ ) Weight ( $0.14$ , $p = 0.28$ ) BMI ( $0.19$ , $p = 0.15$ )	Age ( $p = 0.004$ ), adj. $R^2 = 0.11$
CV <sub>M:Gas</sub>	0.25 [0.22, 0.31]	Age ( $-0.06$ , $p = 0.65$ ) Height ( $0.56$ , $p < 0.0001$ )* Weight ( $0.52$ , $p < 0.0001$ )* BMI ( $0.13$ , $p = 0.34$ )	Sex ( $p < 0.0001$ ), adj. $R^2 = 0.44$
$T_2^*$ <sub>Gas</sub> (ms)	19.9 [17.9, 22.1]	Age ( $-0.12$ , $p = 0.34$ ) Height ( $-0.12$ , $p = 0.37$ ) Weight ( $-0.25$ , $p = 0.06$ ) BMI ( $-0.29$ , $p = 0.02$ )*	BMI ( $p < 0.02$ ), adj. $R^2 = 0.09$
$T_2^*$ <sub>M</sub> (ms)	2.32 [2.26, 2.39]	Age ( $0.34$ , $p = 0.006$ )* Height ( $-0.10$ , $p = 0.44$ ) Weight ( $0.10$ , $p = 0.43$ ) BMI ( $0.21$ , $p = 0.10$ )	Age ( $p = 0.004$ ) and Sex ( $p = 0.004$ ), adj. $R^2 = 0.24$
$T_2^*$ <sub>RBC</sub> (ms)	1.91 [1.84, 1.97]	Age ( $0.60$ , $p < 0.0001$ )* Height ( $0.11$ , $p = 0.38$ ) Weight ( $0.36$ , $p = 0.004$ )* BMI ( $0.37$ , $p = 0.004$ )*	Age ( $p < 0.0001$ ) and weight ( $p = 0.005$ ), adj. $R^2 = 0.41$
M chemical shift in ppm	197.8 [197.7, 198.1]	Age ( $-0.23$ , $p = 0.08$ ) Height ( $0.36$ , $p = 0.004$ )* Weight ( $0.36$ , $p = 0.005$ )* BMI ( $0.15$ , $p = 0.24$ )	Sex ( $p < 0.0001$ ), adj. $R^2 = 0.24$
RBC chemical shift in ppm	216.9 [216.6, 217.2]	Age ( $0.15$ , $p = 0.26$ ) Height ( $0.30$ , $p = 0.02$ )* Weight ( $0.18$ , $p = 0.17$ ) BMI ( $-0.03$ , $p = 0.84$ )	Sex ( $p = 0.001$ ), adj. $R^2 = 0.16$

Note: M and RBC chemical shift are expressed in ppm from the gas frequency reference.

**FIGURE 3** Linear correlation of RBC:M with age in the 62 subjects split according to sex (26 M, 36 F) (A) and the corresponding z-score (B) derived from the linear regression models of (A). Linear correlation of RBC:Gas (C) and  $CV_{RBC:M}$  with age (D).



third column of Table 2 when applying the multiple linear regression analysis (fourth column). BMI and age were also dependent variables and demonstrated a significant correlation ( $p = 0.029$ ).

### 3.3 | Regional gas exchange analyses

Regional differences of the global average xenon gas exchange ratios between the posterior and anterior, inferior middle and superior and proximal and distal lung zones are displayed in Figure 4. Although the gravity dependence (higher signal in the posterior than in the anterior lungs) was clearly present on each individual Gas, M, and RBC image, the regional differences were much more pronounced for RBC and M when compared to gas. Hence, a significant anterior–posterior difference was still observed for the M:Gas and RBC:Gas ratios. There was no significant difference between the anterior and posterior RBC:M values. Additionally, the correlations of RBC:M and RBC:Gas with age were stronger when using average values from the posterior lung compared to the global whole lung values.

All xenon gas exchange ratios were significantly different in the inferior part of the lungs when compared to the middle and superior zones, while there was no significant difference between the middle and superior lung regions. The RBC signal was significantly higher in the middle zone likely due to the higher density of pulmonary veins and vasculature, which was confirmed by the significantly

higher observed RBC:M and RBC:Gas values in the proximal region (defined as an ellipsoid centered on the center of mass of the lung mask and with radii equivalent to  $0.79 \times$  the whole lung mask radii) compared to the distal part of the lung.

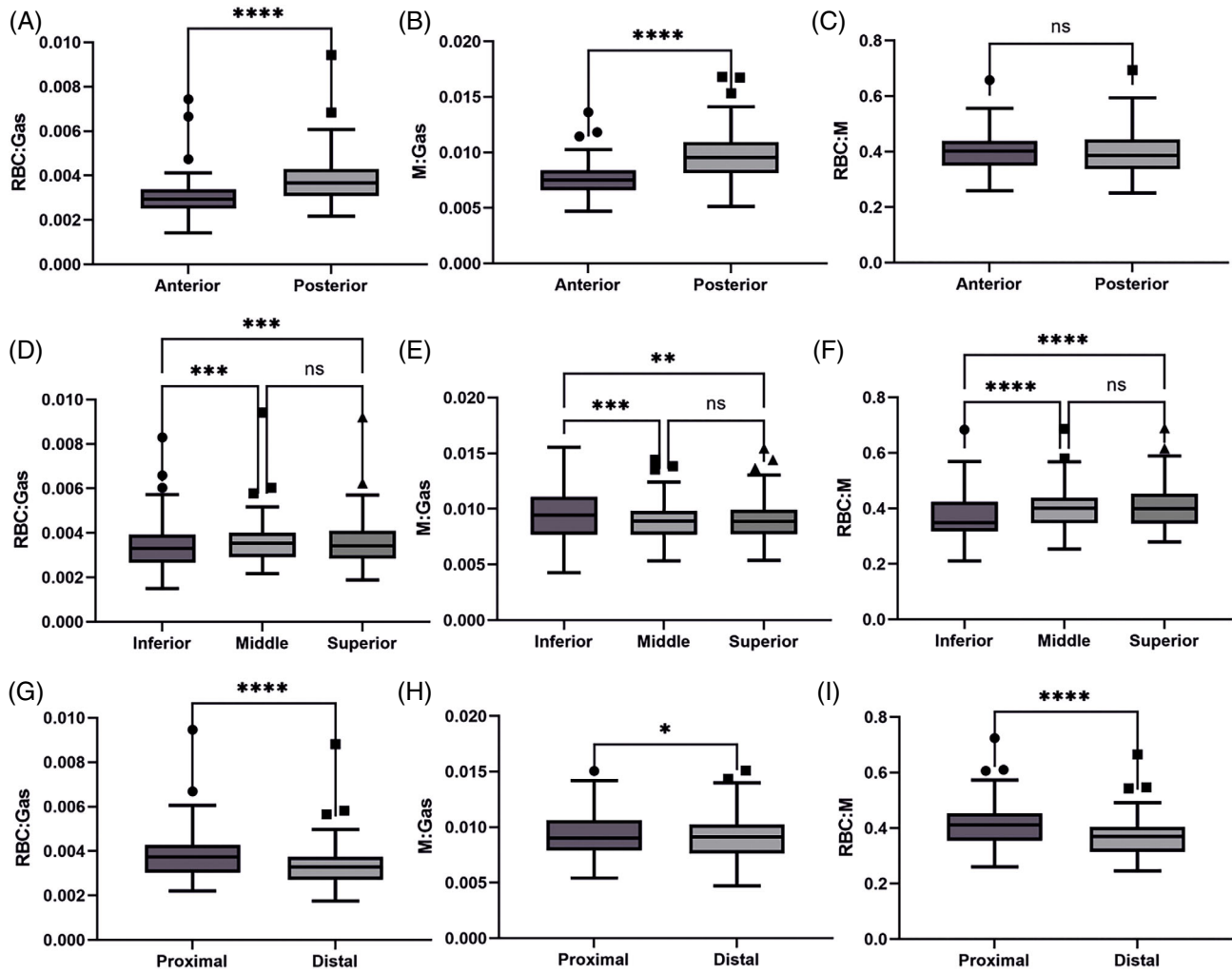
### 3.4 | Lung volume dependence

Table 3 summarizes the xenon imaging markers at the two lung volumes. Gas exchange imaging ratios were all significantly lower at TLC when compared to EIVt with RBC:M, RBC:Gas and M:Gas being on average 8.6%, 33.3% and 39.4% lower, respectively (see Figure 5). There was no significant difference in RBC:Osc. The percentage change in M:Gas between EIVt and TLC was the only parameter significantly correlated with age (Spearman  $r = 0.47$ ,  $p = 0.005$ ) with less reduction of M:gas with lung volume as age increases. The differences in regional values observed and described above at EIVt were all still present at TLC.

## 4 | DISCUSSION

To our knowledge, this is the largest study of healthy volunteers with HP dissolved  $^{129}\text{Xe}$  spectroscopic imaging metrics to be published to date. The main result of this study is the definition of sex and age corrected reference values for RBC:M and RBC:Gas over the age range of 20–70 that can be used to help define the limit of normality for





**FIGURE 4** Box plots of regional gas exchange ratios RBC:Gas (A, D, G), M:Gas (B, E, H) and RBC:M (C, F, I). The lungs were divided into two zones Anterior/Posterior (A, B, C), three zones Inferior/Middle/Superior (D, E, F) and two zones Proximal/Distal (G, H, I). Results of Wilcoxon matched pairs signed rank tests and one way ANOVA paired Friedman tests with Dunn's multiple comparison are expressed as follows:  $p > 0.05$  (ns),  $p < 0.05$  (\*),  $p < 0.01$  (\*\*),  $p < 0.001$  (\*\*\*), and  $p < 0.0001$  (\*\*\*\*).

**TABLE 3** Comparison of dissolved  $^{129}\text{Xe}$  imaging results at two lung volume: EIVt and TLC in a subset of 34 subjects (female/male = 19/15, age = 50 y [37, 56])

Lung volume	EIVt	TLC	Wilcoxon paired <i>t</i> -test <i>p</i> -value
RBC:M	0.38 [0.34, 0.43]	0.35 [0.31, 0.40]	<0.0001
RBC:Gas	0.0036 [0.0030, 0.0041]	0.0022 [0.0020, 0.0025]	<0.0001
M:Gas	0.0093 [0.0079, 0.0105]	0.0062 [0.0058, 0.0070]	<0.0001
RBC:Osc	13.1% [11.6, 15.2%]	12.9% [12.0, 20.7%]	0.07
$T_2^*$ Gas	20.0 ms [17.9, 22.2]	21.5 ms [19.8, 24.5]	<0.0001
$T_2^*$ M	2.33 ms [2.25, 2.39]	2.21 ms [2.12, 2.26]	<0.0001
$T_2^*$ RBC	1.94 ms [1.86, 1.97]	1.85 ms [1.79, 1.89]	<0.0001
M chemical shift in ppm	197.8 [197.7, 198.1]	197.6 [197.5, 197.9]	<0.0001
RBC chemical shift in ppm	216.9 [216.7, 217.2]	216.9 [216.5, 217.1]	0.05

Note: All results are given as median and first and third quartiles [Q1, Q3].

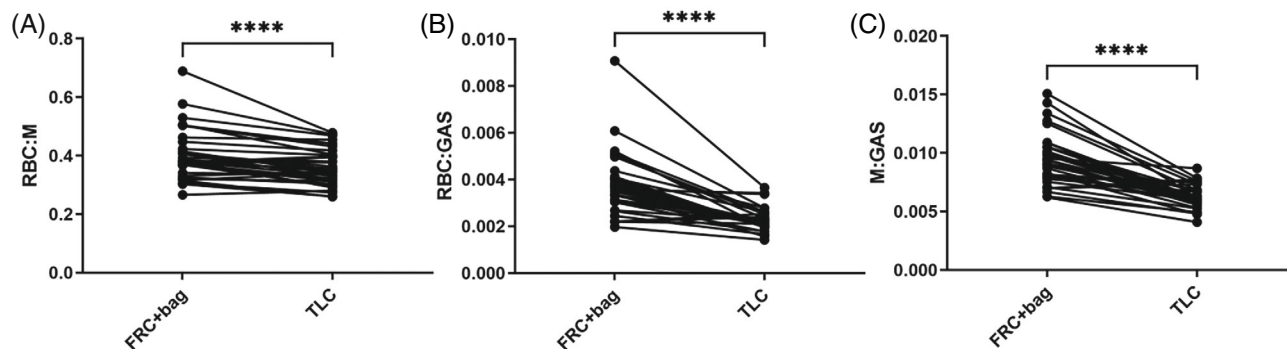


FIGURE 5 Comparison of global gas transfer measurement (RBC:M [A], RBC:Gas [B], M:Gas [C]) measured with dissolved  $^{129}\text{Xe}$  imaging in 34 healthy subjects at two lung volumes (FRC, functional residual capacity; TLC, total lung capacity).

dissolved  $^{129}\text{Xe}$  gas exchange imaging results. Our data confirm that there is a significant age dependence with decreasing  $^{129}\text{Xe}$  imaging gas transfer metrics with increasing age in an adult population, as previously reported by Plummer et al.<sup>22</sup> It is also in agreement with the GLI reference values for  $T_{\text{LCO}}$ .<sup>19</sup> Moreover, our study highlights the significant difference between sexes for  $^{129}\text{Xe}$  transfer into the blood (RBC:M and RBC:Gas) and it includes weight, height, and BMI and reports on the influence of these demographics on a more comprehensive set of  $^{129}\text{Xe}$  imaging parameters such as  $T_2^*$ , frequency shifts, image ratio heterogeneity (CV), regional values and lung volume. With  $^{129}\text{Xe}$  lung MRI entering clinical practice<sup>27</sup> and conclusions about lung pathophysiology, disease progression, and treatment response being drawn from these metrics, it is important to have well-defined healthy reference values when making a clinical interpretation of these metrics. The literature provides recent examples of how significant the results of this study could be for the HP  $^{129}\text{Xe}$  pulmonary imaging community. For example, in a recent journal editorial<sup>16</sup> we raised the possibility that the results of a study demonstrating significant differences in xenon gas transfer measurement between healthy controls and patients with post-acute COVID-19 syndrome<sup>28</sup> could have been different if the groups had been age-matched. Similarly for lung volume, Garrison et al.<sup>24</sup> demonstrated that significant differences in M:Gas and RBC:Gas between subjects with COPD and healthy controls were largely eliminated upon correction for lung-volume contribution.

In this study, we have observed a significantly lower  $^{129}\text{Xe}$  gas-exchange in females when compared to males. This aligns with the GLI reference equations for  $T_{\text{LCO}}$ , as is the near linear decrease of gas exchange with age (above the age of 20 y), which justifies the regression model used in this work. In terms of comparison to data from other centers, the global xenon imaging ratios are expected to be mostly dependent on imaging parameters such as flip angle, repetition time and possibly B0 field

strength but should theoretically be less dependent upon the imaging technique itself. The 1-point Dixon imaging technique is based on acquiring data at an echo time for which the RBC and membrane signals are 90 degrees out of phase, while the chemical shift separation performed in this work is based on acquiring four echoes to recover three unknown signals through matrix inversion. Our method is performed in k-space while the 1-point Dixon is performed in image space and includes additional steps of phase correction. It is therefore possible that the images themselves might be somewhat different in terms of regional signal distribution and further comparative work is warranted. However, global imaging ratios result mostly from the signals in the center of k-space where both techniques have the highest probability to perform best. The results obtained here using a four-echo radial flyback MRI sequence should therefore be applicable to other imaging centers that follow the imaging recommendations of the  $^{129}\text{Xe}$  MRI clinical trial consortium.<sup>18</sup> It is difficult to directly compare our results with the ones published by Plummer et al.<sup>22</sup> in part due to the differences in age range, but mainly due to differences in data analysis and the model applied to their data. While a GAMLSS model with a cubic-regression spline is suitable for fitting highly non-linear data such as  $^{129}\text{Xe}$  gas exchange measurements from childhood to adulthood, it is preferable to apply a model with less fitting parameters when dealing with a near linear trend and a modest amount of data points, as is the case in this study. Another multiple linear regression model of normative  $^{129}\text{Xe}$  imaging metrics from healthy volunteers has been recently reported using a 1-point Dixon imaging method.<sup>29</sup> The study included 37 subjects from the age of 19–87 y and also showed that age and sex were significant predictors, that male sex was associated with an RBC:M increase of 0.17 and that each additional 10 years of age was associated with a decrease of 0.02. These findings are consistent with the values obtained in our study, with our model predicting a

10-year decrease in RBC:M of 0.024 and a smaller RBC:M difference of 0.07 between men and women.

Despite being the largest known population of healthy volunteer data published with dissolved xenon spectroscopic imaging to date, the main limitation of our study is still the relatively small size of the cohort and the inclusion of former smokers. Out of the 62 subjects, none were current smokers nor have known respiratory conditions but 13 had a recorded previous smoking history within the range of 0.01–8.5 pack years and a study comparing age matched smokers and never smokers is therefore warranted. With regard to the size of the cohort, predictive equations are usually derived in pulmonary physiology from the collection of thousands of data sets, which enables the detection of more subtle changes with additional demographics. It is therefore possible that subject height, which is a significant predictor for both  $T_{LCO}$  and  $K_{CO}$ , has not been identified as significant in this study due to sample size. More importantly, the derivation of normality using z-scores usually requires using standard deviation values that depend on subject age and sex. To ensure simplicity and to accommodate the study's limited sample size, male and female data were treated separately with standard deviations of the percent predicted values employed to define the z-scores across the full age range. Consequently, the suggested predicted equations and z-scores should serve as a helpful guide for interpreting  $^{129}\text{Xe}$  imaging results. These equations however should not be applied to a younger age range (less than 20 y). The spread of data for  $T_{LCO}$  and  $K_{CO}$  exhibit distinct age-related patterns during childhood related to the rapid growth and development of the lungs.<sup>19</sup> Plummer et al. have also demonstrated that RBC:Gas and RBC:M increases in children,<sup>22</sup> and needed to apply a generalized additive model to assess the effect of age from childhood to adulthood. A different set of predictive equations should therefore be applied for children's lungs.

The decrease of RBC:Gas and RBC:M with age but relatively stable M:Gas values over the whole age range has been previously reported by Mummy et al.<sup>29</sup> who suggested that the main reason for an age-related decline is the change in RBC signal. The increased heterogeneity of RBC:M and RBC:Gas maps ( $CV_{RBC:M}$  and  $CV_{RBC:Gas}$ ) reported in the present study, along with reduced RBC signal with age suggests RBC signal decreases heterogeneously within the lung as individuals age. A parallel can be drawn with the effect of aging on  $^{129}\text{Xe}$  diffusion images. Fain et al.<sup>30</sup> demonstrated an increase in ADC, and therefore a change in lung microstructure, in a cohort of 44 healthy adult subjects with no smoking history over the age range of 18–69 y. In this latter work, the authors hypothesized that the age-related change in ADC was due to a decrease in alveolar surface area and an increase in

lung compliance similar to mild emphysema. Most of the changes observed in pulmonary function of the aging lung stem from a gradual decrease in lung elastic recoil<sup>31</sup> and the decline in  $T_{LCO}$  is due to a fall in rate constant of carbon monoxide due to alveolar capillaries ( $K_{CO}$ ) more than a fall in alveolar volume.<sup>32</sup> The decline in  $K_{CO}$  may be due to a loss of capillary density caused by subtle changes in alveolar structure associated with the decrease in elastic recoil.<sup>33</sup> Our results are in agreement with this hypothesis and the relatively stable M:Gas measurements with age, suggest an increase in lung compliance rather than emphysematous change.

With regard to the regional differences of the distribution of  $^{129}\text{Xe}$  gas-exchange metrics within the lung, the lack of gravitational dependence of RBC:M values in the anterior–posterior direction is in contradiction with the trend observed in three healthy subjects with xenon transfer contrast imaging methods<sup>12</sup> but agrees with results published by Qing et al.<sup>9</sup> who used a multi-echo IDEAL imaging sequence, in five healthy subjects. This suggests that the tissue and pulmonary vasculature are equally distributed along the anterior/posterior direction. The strong gravity dependence of RBC:gas and M:Gas however is in good agreement with the results reported by Wang et al.<sup>34,35</sup> with a single point Dixon imaging sequence, and can be explained by the increased tissue and capillary densities in the gravitationally dependent lung.<sup>36</sup> Similarly, the higher RBC signal in the proximal part of the lung results from a higher concentration of pulmonary veins and blood volume in this region while the differences observed in the basal/apical direction are in agreement with previously published results.<sup>3,34</sup> The lower RBC:Gas and RBC:M values observed in the inferior part could be explained by the RBC signal being smaller in this region; a trend opposing that of lung ventilation and tissue density in the supine position.

Regarding the effect of lung volume, our results confirm that the lung inflation state has a dramatic impact on the  $^{129}\text{Xe}$  gas exchange measurement, with blood transfer and membrane uptake changing by ~35% between EIVt and TLC. This change can be explained by the difference of lung tissue and blood density between EIVt and TLC and our results are in good agreement with Garisson et al.<sup>24</sup> who also demonstrated a strong linear correlation between the relative changes in xenon gas transfer and the relative changes in lung volume. It further supports the benefit of titrating the administered xenon dose according to subject lung volume and coaching the subjects to ensure that imaging is performed at a controlled lung volume in order to minimize potential measurement errors. The latest recommendation within the HP  $^{129}\text{Xe}$  pulmonary MR imaging community is to use the subject measured (or predicted) TLC or forced vital capacity lung

volumes to derive individual dose volume.<sup>18</sup> A limitation in this study is that simpler height brackets (see Table S1 in supplementary material) were used that did not discriminate between male and female subjects. This table was first introduced by our group in Smith et al.<sup>37</sup> as a means to correct for lung volume differences based on the principle that height is a significant predictor of functional residual capacity. Throughout the 3-y recruitment period, the dosing chart remained the same for consistency, although we acknowledge that it was more granular than the currently recommended approach and the potential biases it may have introduced. Likewise, we acknowledge the absence of hematocrit recording in our study design, as adjustments for hemoglobin are becoming recognized in <sup>129</sup>Xe gas exchange MRI.<sup>38</sup> Furthermore, a potential confounding variable contributing to the observed sex and age dependence in this study is the menstrual cycle, as Sansores et al.<sup>39</sup> have shown its impact on pulmonary carbon monoxide diffusing capacity. Our study's ethics protocol did not encompass the documentation of pre- versus post-menopausal status, anemia, or menstrual cycles, necessitating further investigation.

Among the <sup>129</sup>Xe gas exchange metrics, RBC:M had the lowest variability with lung volume, making it less susceptible to measurement error due to incorrect breathing maneuver, and it was also the most reproducible imaging parameter with an intra-session ICC of 0.983 (and a 95% confidence interval of 0.924–0.996). The lower reproducibility of RBC:Gas and M:Gas measurements when compared to RBC:M has previously been reported by Kern et al.<sup>40</sup> who assessed <sup>129</sup>Xe gas exchange ratios with a CSSR imaging technique. The authors found that RBC:M and the septal thickness were robust and sensitive markers of gas exchange and hypothesized that lung volume was the major source of RBC:Gas and M:Gas measurement variability. The reproducibility of functional metrics of HP dissolved-phase <sup>129</sup>Xe MRI has also been assessed by Hahn et al.<sup>23</sup> using a 1-point Dixon sequence. Here also, coefficient of variation and ICC were significantly better for RBC:M (11.5% and 0.92) compared to RBC:Gas (19.2% and 0.78) and M:Gas (20.0% and 0.79).

A major limitation in our reproducibility sub-study is the small sample size of eight subjects. While the 95% confidence interval for ICC of RBC:M and M:Gas is good, the results for the other imaging metrics are less conclusive. A significant bias is observed for RBC:Gas and M:Gas, which we attribute to the small sample size. The Bland–Altman plot of inter- and intra-session RBCOsc shows a large variability between the measurements; however, to the best of our knowledge the reproducibility of RBCOsc has not been reported elsewhere. More generally, the change in the sequence parameters (shorter TR and smaller flip angle) to match the xenon trial consortium

recommendation had a negative impact on the SNR of the RBC k-space center signal when compared to previously published results.<sup>3</sup> Additional filtering of the time evolution of the RBC signal or measuring RBCOsc more reliably with an independent spectroscopy sequence<sup>13</sup> may be needed to improve RBC SNR.


## 5 | CONCLUSIONS

In conclusion, dissolved <sup>129</sup>Xe MRI gas transfer metrics in healthy volunteers depend upon sex, age, and lung volume. <sup>129</sup>Xe gas transfer decreases with age and with increasing lung volume, suggesting that correction and control of lung volume are necessary for the correct interpretation of these metrics. These data could be used to allow comparison of groups of subjects with different demographics in a clinical study or, as we currently do in our imaging center, help clinicians interpret <sup>129</sup>Xe imaging results for clinical diagnosis by producing percent predicted values and/or z-scores.

## ACKNOWLEDGMENTS

We thank Matt Willmering, Bastiaan Driehuys and David Mummy for interesting discussions on age and sex dependent <sup>129</sup>Xe related findings. The work was funded by MRC grant MR/M008894/1, EPSRC EP/X025187/1, NIHR grant: COV-LT2-0049 and the Sheffield NIHR biomedical research center. The views expressed are those of the authors and not necessarily those of the EPSRC, MRC, the NIHR or the Department of Health and Social Care.

## ORCID

Guilhem J. Collier  <https://orcid.org/0000-0002-1874-4775>

Laura C. Saunders  <https://orcid.org/0000-0002-1080-9861>

Neil J. Stewart  <https://orcid.org/0000-0001-8358-394X>

Graham Norquay  <https://orcid.org/0000-0002-4108-9035>

Paul J. C. Hughes  <https://orcid.org/0000-0002-7979-5840>

A. A. Roger Thompspon  <https://orcid.org/0000-0002-0717-4551>

## REFERENCES

- Norquay G, Collier GJ, Rodgers OI, Gill AB, Sreaton NJ, Wild J. Standalone portable xenon-129 hyperpolariser for multicentre clinical magnetic resonance imaging of the lungs. *Br J Radiol.* 2022;95:20210872.
- Kaushik SS, Robertson SH, Freeman MS, et al. Single-breath clinical imaging of hyperpolarized <sup>129</sup>Xe in the airspaces, barrier, and red blood cells using an interleaved 3D radial 1-point Dixon acquisition. *Magn Reson Med.* 2016;75:1434-1443.

3. Collier GJ, Eaden JA, Hughes PJC, et al. Dissolved  $^{129}\text{Xe}$  lung MRI with four-echo 3D radial spectroscopic imaging: quantification of regional gas transfer in idiopathic pulmonary fibrosis. *Magn Reson Med.* 2021;85:2622-2633.
4. Qing K, Tustison NJ, Mugler JP 3rd, et al. Probing changes in lung physiology in COPD using CT, perfusion MRI, and hyperpolarized Xenon-129 MRI. *Acad Radiol.* 2019;26:326-334.
5. Wang Z, Bier EA, Swaminathan A, et al. Diverse cardiopulmonary diseases are associated with distinct xenon magnetic resonance imaging signatures. *Eur Respir J.* 2019;54:1900831.
6. Grist JT, Chen M, Collier GJ, et al. Hyperpolarized  $^{129}\text{Xe}$  MRI abnormalities in dyspneic participants 3 months after COVID-19 pneumonia: preliminary results. *Radiology.* 2021;301:E353-E360.
7. Matheson AM, McIntosh MJ, Kooner HK, et al. Persistent  $^{129}\text{Xe}$  MRI pulmonary and CT vascular abnormalities in symptomatic individuals with post-acute COVID-19 syndrome. *Radiology.* 2022;305:466-476.
8. Saunders LC, Collier GJ, Chan HF, et al. Longitudinal lung function assessment of patients hospitalized with COVID-19 using  $^1\text{H}$  and  $^{129}\text{Xe}$  lung MRI. *Chest.* 2023;164:700-716.
9. Qing K, Ruppert K, Jiang Y, et al. Regional mapping of gas uptake by blood and tissue in the human lung using hyperpolarized xenon-129 MRI. *J Magn Reson Imaging.* 2014;39:346-359.
10. Kammerman J, Hahn AD, Cadman RV, Malkus A, Mummy D, Fain SB. Transverse relaxation rates of pulmonary dissolved-phase hyperpolarized  $^{129}\text{Xe}$  as a biomarker of lung injury in idiopathic pulmonary fibrosis. *Magn Reson Med.* 2020;84:1857-1867.
11. Collier GJ, Schulte RF, Rao M, Norquay G, Ball J, Wild JM. Imaging gas-exchange lung function and brain tissue uptake of hyperpolarized  $^{129}\text{Xe}$  using sampling density-weighted MRSI. *Magn Reson Med.* 2023;89:2217-2226.
12. Amzajerjian F, Ruppert K, Hamedani H, et al. Measuring pulmonary gas exchange using compartment-selective xenon-polarization transfer contrast (XTC) MRI. *Magn Reson Med.* 2021;85:2709-2722.
13. Bier EA, Robertson SH, Schrank GM, et al. A protocol for quantifying cardiogenic oscillations in dynamic  $^{129}\text{Xe}$  gas exchange spectroscopy: the effects of idiopathic pulmonary fibrosis. *NMR Biomed.* 2019;32:e4029.
14. Ruppert K, Altes TA, Mata JF, Ruset IC, Hersman FW, Mugler JP 3rd. Detecting pulmonary capillary blood pulsations using hyperpolarized xenon-129 chemical shift saturation recovery (CSSR) MR spectroscopy. *Magn Reson Med.* 2016;75:1771-1780.
15. Norquay G, Leung G, Stewart NJ, Wolber J, Wild JM.  $^{129}\text{Xe}$  chemical shift in human blood and pulmonary blood oxygenation measurement in humans using hyperpolarized  $^{129}\text{Xe}$  NMR. *Magn Reson Med.* 2017;77:1399-1408.
16. Wild JM, Collier G.  $^{129}\text{Xe}$  pulmonary MRI for individuals with post-acute COVID-19 syndrome. *Radiology.* 2022;305:477-478.
17. Ruppert K, Amzajerjian F, Hamedani H, et al. Assessment of flip angle-TR equivalence for standardized dissolved-phase imaging of the lung with hyperpolarized  $^{129}\text{Xe}$  MRI. *Magn Reson Med.* 2018;81:1784-1794.
18. Niedbalski PJ, Hall CS, Castro M, et al. Protocols for multi-site trials using hyperpolarized  $^{129}\text{Xe}$  MRI for imaging of ventilation, alveolar-airspace size, and gas exchange: a position paper from the  $^{129}\text{Xe}$  MRI clinical trials consortium. *Magn Reson Med.* 2021;86:2966-2986.
19. Stanojevic S, Graham BL, Cooper BG, et al. Official ERS technical standards: global lung function initiative reference values for the carbon monoxide transfer factor for Caucasians. *Eur Respir J.* 2017;50:1700010.
20. Wang Z, Rankine L, Bier EA, et al. Using hyperpolarized  $^{129}\text{Xe}$  gas-exchange MRI to model the regional airspace, membrane, and capillary contributions to diffusing capacity. *J Appl Physiol (1985).* 2021;130:1398-1409.
21. Stewart NJ, Leung G, Norquay G, et al. Experimental validation of the hyperpolarized  $^{129}\text{Xe}$  chemical shift saturation recovery technique in healthy volunteers and subjects with interstitial lung disease. *Magn Reson Med.* 2015;74:196-207.
22. Plummer JW, Willmering MM, Cleveland ZI, Towe C, Woods JC, Walkup LL. Childhood to adulthood: accounting for age dependence in healthy-reference distributions in  $^{129}\text{Xe}$  gas-exchange MRI. *Magn Reson Med.* 2023;89:1117-1133.
23. Hahn AD, Kammerman J, Evans M, et al. Repeatability of regional pulmonary functional metrics of hyperpolarized  $^{129}\text{Xe}$  dissolved-phase MRI. *J Magn Reson Imaging.* 2019;50:1182-1190.
24. Garrison WJ, Qing K, He M, et al. Lung volume dependence and repeatability of hyperpolarized  $^{129}\text{Xe}$  MRI gas uptake metrics in healthy volunteers and participants with COPD. *Radiol Card Imaging.* 2023;5:e220096.
25. Norquay G, Collier GJ, Rao M, Stewart NJ, Wild JM.  $^{129}\text{Xe}$ -Rb spin-exchange optical pumping with high photon efficiency. *Phys Rev Lett.* 2018;121:153201.
26. Kaushik SS, Freeman MS, Yoon SW, et al. Measuring diffusion limitation with a perfusion-limited gas—hyperpolarized  $^{129}\text{Xe}$  gas-transfer spectroscopy in patients with idiopathic pulmonary fibrosis. *J Appl Physiol.* 2014;117:577-585.
27. Stewart NJ, Smith LJ, Chan HF, et al. Lung MRI with hyperpolarised gases: current & future clinical perspectives. *Br J Radiol.* 2021;95:20210207.
28. Adalsteinsson E, Irrazabal P, Topp S, Meyer C, Macovski A, Spielman DM. Volumetric spectroscopic imaging with spiral-based k-space trajectories. *Magn Reson Med.* 1998;39:889-898.
29. Mummy D. *Hyperpolarized  $^{129}\text{Xe}$  MRI and spectroscopy in healthy control subjects reveals age-related changes in measurements of pulmonary gas exchange* 2022. In *Proceedings of the 31st Annual Meeting of ISMRM*, London, UK, 2022. abstract 1168.
30. Fain SB, Altes TA, Panth SR, et al. Detection of age-dependent changes in healthy adult lungs with diffusion-weighted  $^3\text{He}$  MRI. *Acad Radiol.* 2005;12:1385-1393.
31. Pride NB. Ageing and changes in lung mechanics. *Eur Respir J.* 2005;26:563-565.
32. Hughes JMB. *Physiology and Practice of Pulmonary Function*. Association for Respiratory Technology & Physiology; 2009.
33. Hughes JM, Pride NB. Examination of the carbon monoxide diffusing capacity (DL(CO)) in relation to its KCO and VA components. *Am J Respir Crit Care Med.* 2012;186:132-139.
34. Wang Z, Robertson SH, Wang J, et al. Quantitative analysis of hyperpolarized  $^{129}\text{Xe}$  gas transfer MRI. *Med Phys.* 2017;44:2415-2428.
35. Wang JM, Robertson SH, Wang Z, et al. Using hyperpolarized  $^{129}\text{Xe}$  MRI to quantify regional gas transfer in idiopathic pulmonary fibrosis. *Thorax.* 2018;73:21-28.
36. West JB, Matthews FL. Stresses, strains, and surface pressures in the lung caused by its weight. *J Appl Physiol.* 1972;32:332-345.

37. Smith LJ, Collier GJ, Marshall H, et al. Patterns of regional lung physiology in cystic fibrosis using ventilation magnetic resonance imaging and multiple-breath washout. *Eur Respir J*. 2018;52:1800821.
38. Bechtel A, Lu J, Mummy D, et al. Establishing a hemoglobin adjustment for  $^{129}\text{Xe}$  gas exchange MRI and MRS. *Magn Reson Med*. 2023;90:1555-1568.
39. Sansores RH, Abboud RT, Kennell C, Haynes N. The effect of menstruation on the pulmonary carbon monoxide diffusing capacity. *Am J Respir Crit Care Med*. 1995;152:381-384.
40. Kern AL, Gutberlet M, Qing K, et al. Regional investigation of lung function and microstructure parameters by localized  $^{129}\text{Xe}$  chemical shift saturation recovery and dissolved-phase imaging: a reproducibility study. *Magn Reson Med*. 2019;81:13-24.

### SUPPORTING INFORMATION

Additional supporting information may be found in the online version of the article at the publisher's website.

**Table S1.**  $^{129}\text{Xe}$  dose volume for dissolved xenon imaging according to patient height.

**Table S2.** Patient demographics and imaging results sorted by sex and decade.

**Table S3.** Patient demographics sorted by decade for the 34 subjects who underwent dissolved xenon imaging at both EIVt and TLC.

**Table S4.** Patient demographics for the 8 subjects who participated in the reproducibility study.

**How to cite this article:** Collier GJ, Smith LJ, Saunders LC, et al. Age, sex, and lung volume dependence of dissolved xenon-129 MRI gas exchange metrics. *Magn Reson Med*. 2024;1-13. doi: 10.1002/mrm.30133